Received: 16 October 2024 | Revised: 3 March 2025 | Accepted: 3 March 2025

DOI: 10.1002/alz.70126

Alzheimer's & Dementia®
THE JOURNAL OF THE ALZHEIMER'S ASSOCIATION

RESEARCH ARTICLE

Microstructural assessment of the locus coeruleus–entorhinal cortex pathway and association with ATN markers in cognitive impairment

Marco Aiello[1] | **Moira Marizzoni**[2] | **Pasquale Borrelli**[1] | **Carlo Cavaliere**[1] | **Federica Ribaldi**[3,4] | **Valentina Garibotto**[5,6,7] | **Max Scheffler**[8] | **Ileana O. Jelescu**[9] | **Jorge Jovicich**[10] | **Marco Catani**[1] | **Marco Salvatore**[1] | **Giovanni B. Frisoni**[3,4] | **Michela Pievani**[11]

[1]IRCCS SYNLAB SDN, Naples, Italy

[2]Biological Psychiatry Unit, IRCCS Istituto Centro San Giovanni di Dio Fatebenefratelli, Brescia, Italy

[3]Laboratory of Neuroimaging of Aging (LANVIE), University of Geneva, Geneva, Switzerland

[4]Geneva Memory Center, Department of Rehabilitation and Geriatrics, Geneva University Hospitals, Geneva, Switzerland

[5]Laboratory of Neuroimaging and Innovative Molecular Tracers (NIMTlab), Geneva University Neurocenter and Faculty of Medicine, University of Geneva, Geneva, Switzerland

[6]Division of Nuclear Medicine and Molecular Imaging, Geneva University Hospitals, Geneva, Switzerland

[7]CIBM Center for Biomedical Imaging, Geneva, Switzerland

[8]Division of Radiology, Geneva University Hospitals, Geneva, Switzerland

[9]Lausanne University Hospital (CHUV) and University of Lausanne (UNIL), Lausanne, Switzerland

[10]Center for Mind/Brain Sciences, University of Trento, Mattarello, Italy

[11]Laboratory of Alzheimer's Neuroimaging and Epidemiology, IRCCS Istituto Centro San Giovanni di Dio Fatebenefratelli, Brescia, Italy

Correspondence
Marco Aiello, IRCCS SYNLAB SDN, Via Gianturco 113, 80143 Naples, Italy.
Email: marco.aiello@synlab.it

Funding information
Italian Ministry of University and Research; National Recovery and Resilience Plan; MNESYS, Grant/Award Number: PE0000006; Private Foundation of Geneva University Hospitals; A.P.R.A.—Association Suisse pour la Recherche sur la Maladie d'Alzheimer; Fondation Segré; Race Against Dementia Foundation; Fondation Child Care; Fondation Edmond J. Safra; Fondation Minkoff; Fondazione Agusta; McCall Macbain Foundation; Nicole et René Keller; Fondation AETAS; H2020, Grant/Award Number: 667375; Innovative Medicines Initiative,

Abstract

INTRODUCTION: Whether Alzheimer's disease pathology involves white matter pathways connecting the locus coeruleus (LC) to the entorhinal cortex (EC) is unclear. In this cross-sectional observational study, we investigated the microstructural integrity of the LC–EC pathway in relation to amyloid, tau, and neurodegeneration (ATN) biomarkers along the cognitive spectrum from normal cognition to dementia.

METHODS: One hundred twenty-four participants underwent clinical assessment, diffusion-weighted imaging, structural magnetic resonance imaging (N), amyloid (A), and tau (T) positron emission tomography. Diffusivity indices were assessed in the LC–EC tract using a probabilistic atlas, and linear models were used to assess associations with ATN markers and cognition.

RESULTS: Differences in LC–EC microstructural parameters were observed in participants with Braak stage > I versus Braak 0 ($p < 0.020$), N+ versus N– ($p < 0.001$), and

Grant/Award Numbers: 115736, 115952; Swiss National Science Foundation, Grant/Award Numbers: 320030_182772, 320030_185028, 320030_169876; VELUX Foundation; Schmidheiny foundation; Italian Ministry of Health, Grant/Award Numbers: GR-2018-12366779, RicercaCorrente; SNSF Eccellenza, Grant/Award Number: PCEFP2_194260

cognitively impaired versus unimpaired ($p < 0.019$). LC–EC mean diffusivity was associated with Mini-Mental State Examination score even after accounting for ATN markers ($p = 0.015$).

DISCUSSION: Our results suggest that LC–EC diffusivity provides complementary information over ATN biomarkers in explaining cognitive impairment.

KEYWORDS
amyloid/tau/neurodegeneration, dementia, diffusion-weighted imaging, entorhinal cortex, locus coeruleus, magnetic resonance imaging

Highlights

- Locus coeruleus–entorhinal cortex (LC–EC) tract microstructure is associated with tau and especially neurodegeneration markers.
- LC–EC tract microstructure is more sensitive to tau pathology and neurodegeneration than tracts commonly affected in Alzheimer's disease.
- LC–EC diffusivity measures provide complementary information over amyloid, tau, and neurodegeneration (ATN) biomarkers.

1 | BACKGROUND

The locus coeruleus (LC) is the main source of noradrenaline, a neurotransmitter that modulates a wide range of functions, including vigilance, behavior, and cognition.[1,2] LC dysfunction plays an important role in Alzheimer's disease (AD), as documented by in vivo imaging studies reporting associations between LC impairment and memory deficits, neuropsychiatric symptoms, and sleep disturbances.[3–5] According to the revised Braak staging model for AD, the LC is the earliest site showing AD-related changes,[6–8] that is, hyperphosphorylated "pre-tangle" tau that precedes neurofibrillary tangle deposition in the entorhinal and transentorhinal cortices.[8] Due to its extensive projections to forebrain regions vulnerable to AD, such as the entorhinal cortex (EC), the hippocampus, and the neocortex, the LC is a plausible anatomical model for trans-neuronal spreading of tau pathology in a prion-like manner.[9]

Diffusion-weighted imaging (DWI) offers the possibility to assess white matter (WM) fibers connecting the LC to the EC (LC–EC) in vivo by investigating its microstructural properties. Diffusion tensor imaging (DTI) can characterize tissue organization by describing the motion of water molecules through summary parameters such as fractional anisotropy (FA), mean diffusivity (MD), radial diffusivity (RD), and axial diffusivity (AxD).

Reduced FA and increased MD, AxD, and RD are commonly observed in the medial temporal and limbic tracts of AD patients and are interpreted as indicative of axonal loss/degeneration (FA and MD) or demyelination processes (RD).[10–12]

Previous in vivo DWI studies investigating LC–EC tract microstructure in clinical cohorts with AD dementia reported higher RD[13,14] or higher free water[15] in patients compared to cognitively unimpaired controls, supporting the view that diffusivity measures are sensitive to structural changes in this tract. Notably, microstructural patterns observed in cognitively impaired cohorts differ from those observed in normal aging, as recent DWI studies reported lower FA[16] or, surprisingly, lower (rather than higher) MD and RD in cognitively unimpaired older adults.[17] The clinical value of LC–EC microstructure as a marker of cognitive impairment (CI) in clinical populations has yet to be fully explored, as previous studies did not observe reliable associations with cognition.[14,15] Moreover, previous studies detected no difference in LC–EC pathway diffusivity indices generally altered in AD, such as FA, MD, or AxD,[14,15] and abnormalities were more pronounced in patients with behavioral variant frontotemporal dementia,[14] although neuropathological studies have shown that LC impairment occurs later in this disease[18] and is generally less pronounced than in AD.[19,20] Furthermore, we know little about the possible mechanisms underlying LC–EC microstructural alterations in patients with CI, as a comprehensive assessment of its microstructure in relation to AD hallmarks, that is, amyloid (A), tau (T), and neurodegeneration (N), is lacking. To date, only two studies have investigated LC–EC pathway abnormalities in AD patients in relation to neurodegeneration: one reporting an association with plasma markers of axonal damage[15] and the other no association with EC thickness.[14] Neither study investigated A or T markers. One study on normal aging reported a strong association between FA and cerebrospinal fluid (CSF) total tau, a moderate association with phosphorylated tau (p-tau), and no association with amyloid.[21] However, plasma and CSF markers provide only indirect measures of AD pathology, while positron emission tomography (PET) and magnetic resonance imaging (MRI) markers enable the assessment of both the amount and spatial distribution of ATN pathology. This is relevant in the context of LC assessment because previous in vivo LC-sensitive MRI sequences (LC-MRI) and neuropathological evidence showed that LC impairment is associated with tau pathology and

neurodegeneration in early (i.e., EC) and more advanced (i.e., neocortical) Braak stages,[3,6,8,22,23] while associations with amyloid pathology are weaker or conflicting.[24,25]

This study aims to investigate the relationship among LC–EC microstructure, cognition, and ATN biomarkers in patients from a memory clinic. We hypothesized that microstructural alterations of the LC–EC pathway (1) can be detected in patients with CI, (2) are associated with tau pathology (both in the EC and neocortex) and neurodegeneration, and (3) provide meaningful information on CI over ATN biomarkers.

RESEARCH IN CONTEXT

1. **Systematic review**: Relevant literature was reviewed through databases such as PubMed. While a few studies have investigated the microstructural integrity of the locus coeruleus–entorhinal cortex (LC–EC) pathway in Alzheimer's disease (AD), less is known about the relationship between diffusivity measures and amyloid, tau, and neurodegeneration (ATN) markers in memory clinic patients.
2. **Interpretation**: LC–EC microstructure was (a) associated with markers of tau pathology and neurodegeneration in the medial temporal cortex (MTL), (b) associated with cognitive impairment (CI) even after accounting for ATN markers, and (c) more sensitive to tau pathology and neurodegeneration than tracts commonly affected in AD. Overall, these findings suggest that LC–EC diffusivity provides complementary information over ATN biomarkers in explaining CI.
3. **Future directions**: Future studies should investigate (a) longitudinal changes in LC–EC pathway microstructure and their association with cognitive decline, (b) the contribution of other non-AD pathologies to LC–EC microstructure, and (c) exploiting advanced diffusion protocols to enable LC–EC tract-based analysis.

2 | METHODS

This work has been designed as an observational cross-sectional retrospective study. The analysis and reporting are consistent with the Strengthening the Reporting of Observational studies in Epidemiology (STROBE) guidelines for cross-sectional studies.[26]

2.1 | Participants

One hundred twenty-four participants were retrospectively included from the Geneva Memory Clinic (GMC) cohort at Geneva University Hospitals. Participants were classified according to COSCODE (Brain Connectivity and Metacognition in Persons with Subjective Cognitive Decline) clinical workup that includes three visits: (1) cognitive screening using the Mini-Mental State Examination (MMSE), Three-Objects-Three-Places Test, and Clock Drawing Test; (2) comprehensive cognitive assessment; and (3) deep cognitive phenotyping.[27] All cases were discussed in a memory board by a group of clinicians and neuropsychologists. Inclusion criteria were normal cognition (CU) or CI. Exclusion criteria were the presence of psychiatric disorders or vascular dementia. CU participants were recruited among volunteers or patients referring to the memory clinic but showing normal cognition on all cognitive tests, while CI participants were patients with a diagnosis of mild CI or dementia based on current clinical diagnostic criteria.[28,29] For the aims of this study, we included individuals with available clinical data, DWI data, and amyloid PET and tau PET data during the period of recruitment (2014–2019). We included $n = 30$ CU and $n = 94$ CI participants ($n = 80$ mild cognitive impairment [MCI] and $n = 14$ patients with dementia) out of 146 participants with available data. Demographic, clinical, and biomarker information of the sample is summarized in Table 1.

2.2 | Standard protocol approvals, registrations, and patient consents

This study was approved by the local ethics committee and has been conducted in accordance with the principles of the Declaration of Helsinki and the International Conference on Harmonization Good Clinical Practice guidelines. Each participant provided a voluntary written informed consent for retrospective analysis of clinical, biological, and imaging data (PB_2016-01346, 2020-00403).

2.3 | Brain imaging acquisition and processing

2.3.1 | MRI protocol

All subjects underwent MRI exams on a 3 Tesla scanner (Magnetom Skyra, Siemens Healthineers) equipped with 64-channel head coils. The MRI protocol included the following sequences: high-resolution anatomical T1-weighted with isotropic resolution of 0.9 mm, matrix size of 288 × 288 × 208, repetition time (TR) 1930 ms, echo time (TE) 2.36 ms; diffusion-weighted echoplanar spin-echo (DWI) acquired with 30 diffusion directions and a diffusion gradient strength of 1000 s/mm^2, 1 separate volume with a b-value of zero, axial orientation, in-plane resolution of 1 mm, slice thickness of 2 mm, matrix size of 256 × 256 × 72, TR 4200 ms, TE 71 ms.

2.3.2 | DWI processing

Acquired DWI data were pre-processed to correct for potential artifacts. In particular, the images were denoised by applying a

TABLE 1 Baseline demographic and clinical features of the participants included in the study.

	CU $n = 30$	CI $n = 94$	p
Age, years	75 ± 8	76 ± 7	0.516
Sex, N females (%)	18 (60%)	49 (52%)	0.587
Education level, N (%)			**0.048**
Primary	0 (0%)	10 (11%)	
High school	7 (23%)	33 (35%)	
University	23 (77%)	51 (54%)	
MMSE	29 ± 1	25 ± 5	**<0.001**
Clinical stage			
MCI	–	80 (85%)	–
Dementia	–	14 (15%)	–
Amyloid positive, N (%)	7 (23%)	69 (73%)	**<0.001**
Tau positive, N (%)	2 (7%)	49 (52%)	**<0.001**
Neurodegeneration positive, N (%)[a]	4 (13%)	30 (32%)	0.075

Note: Values denote mean ± standard deviation or number (percentage). *P* denotes significance on analysis of variance test for continuous variables and χ^2 test for categorical variables. Amyloid positivity is defined based on visual reading of amyloid PET. Tau positivity is defined as Braak stage ≥ IV on visual reading of flortaucipir PET. Neurodegeneration positivity is defined based on visual assessment of MTL atrophy on Scheltens' scale.
Bold values denote significant differences ($p < 0.05$).
Abbreviations: CI, cognitively impaired; CU, cognitively unimpaired; LC, locus coeruleus; MCI, mild cognitive impairment; MMSE, Mini-Mental State Examination; MTL, medial temporal lobe; PET, positron emission tomography.
[a]Data missing for one subject.

Marchenko–Pastur principal component analysis noise removal technique,[30] and corrected for eddy current–induced distortion and artifacts due to participant movement by an integrated method.[31] For the aforementioned processing steps, a combination of commands from MRtrix[32] (version 3.0.3) and FMRIB-FSL[33] (version 6.0) toolboxes was adopted. In particular, dwidenoise and dwibiascorrect commands of the MRtrix3 toolbox were applied for image denoising and B1 field inhomogeneity correction, respectively. The eddy routine of the FSL software library was used to correct for eddy-current distortion artifacts and participant movements. FA, MD, RD, and AxD parametric maps were derived from the eigenvalues of the diffusion tensor using the tensor2metric command of the MRtrix3 toolbox.

Diffusivity indices were measured in the LC–EC pathway and other tracts using a region of interest (ROI) approach[34] with previously published probabilistic atlases. The LC–EC pathway atlas was derived from the Human Connectome Project data using probabilistic tractography to reconstruct the fibers connecting the seed region (LC) to the EC ROI.[13] Specifically, the atlas includes fibers arising from the LC, entering the thalamus and the amygdala, and reaching the EC. The pathways were reconstructed using a two-stage seeding approach. In the first stage, bundles connecting the LC seed to the amygdala were reconstructed; the output of the first stage was used as a seed to reconstruct the bundles connecting to the EC. In both steps, the thalamus was used as an inclusion ROI and the ventral tegmental areas as exclusion ROI. Voxels with probability values > 0.20 were included and binarized to define the LC–EC ROI.[13] The spatial transformation from the LC–EC pathway mask (Montreal Neurologic Institute[MNI]152 space) to the T1-weighted image was obtained by inverting the combination of linear and non-linear transforms obtained with the FLIRT and FNIRT routines of the FMRIB-FSL software. The following MNI152 template was selected for spatial normalization and accessed with TemplateFlow (23.1.0,@templateflow):ICBM 152 Nonlinear Asymmetrical template version 2009c (@mni152nlin2009casym, RRID:SCR_008796; TemplateFlow ID: MNI152NLin2009cAsym).

Subsequently, the resulting spatially transformed LC pathway masks were registered to the DWI space by applying an affine transformation with 12 degrees of freedom derived from the alignment of the T1-weighted images to DWI images by means of the FLIRT routine. WM, gray matter, and CSF masks were segmented from the anatomical scans with FMRIB's Automated Segmentation Tool (FAST)[35] using three-class segmentation. The CSF masks were spatially transformed from T1-weighted to DWI space with the same affine registration matrix that was used for the LC–EC masks, as outlined above, to mitigate possible CSF contamination in the LC–EC masks before extracting microstructural parameters. Considering that the LC–EC tract follows a tortuous and anatomically complex path, it is important to evaluate the microstructural features along the entire pathway. To this purpose, following an approach similar to previous studies,[15,16] a comparative analysis of microstructural measures on each subject, along a uniform sampling of 30 points from LC to EC along the medial line of the ROI, was performed.

In addition to the LC–EC tract, we assessed five control tracts: two WM tracts known to be affected in dementia patients (i.e., positive control tracts: dorsal and parahippocampal subdivisions of the cingulum) and three tracts relatively spared in AD (i.e., negative control tracts: anterior thalamic radiation, corticospinal tract, and frontopontine tract). The control tracts were extracted from the Johns Hopkins University ICBM-DTI-81 WM tractography probabilistic atlas supplied with the FMRIB-FSL toolbox and a probabilistic atlas of human brainstem pathways.[36] The tracts were spatially transformed from the MNI152 to the DWI space by using the T1-weighted image as the intermediate image and by applying the same routine as for the LC–EC pathway mask. Finally, the averages of DWI parametric maps (FA, MD, RD, and AxD) within each WM tract were calculated. For all tracts, left and right hemispheres were averaged to obtain a single measure to reduce the number of comparisons and because we had no a priori hypothesis on lateralized effects. Figure 1 depicts the above tracts in the MNI152 space.

2.4 | Anatomical scans processing

For each patient, bilateral hippocampal volumes (HVs) and bilateral EC thickness were obtained by applying the cross-sectional recon-all routine from the FreeSurfer package[37] (version 7.2) to the T1-weighted

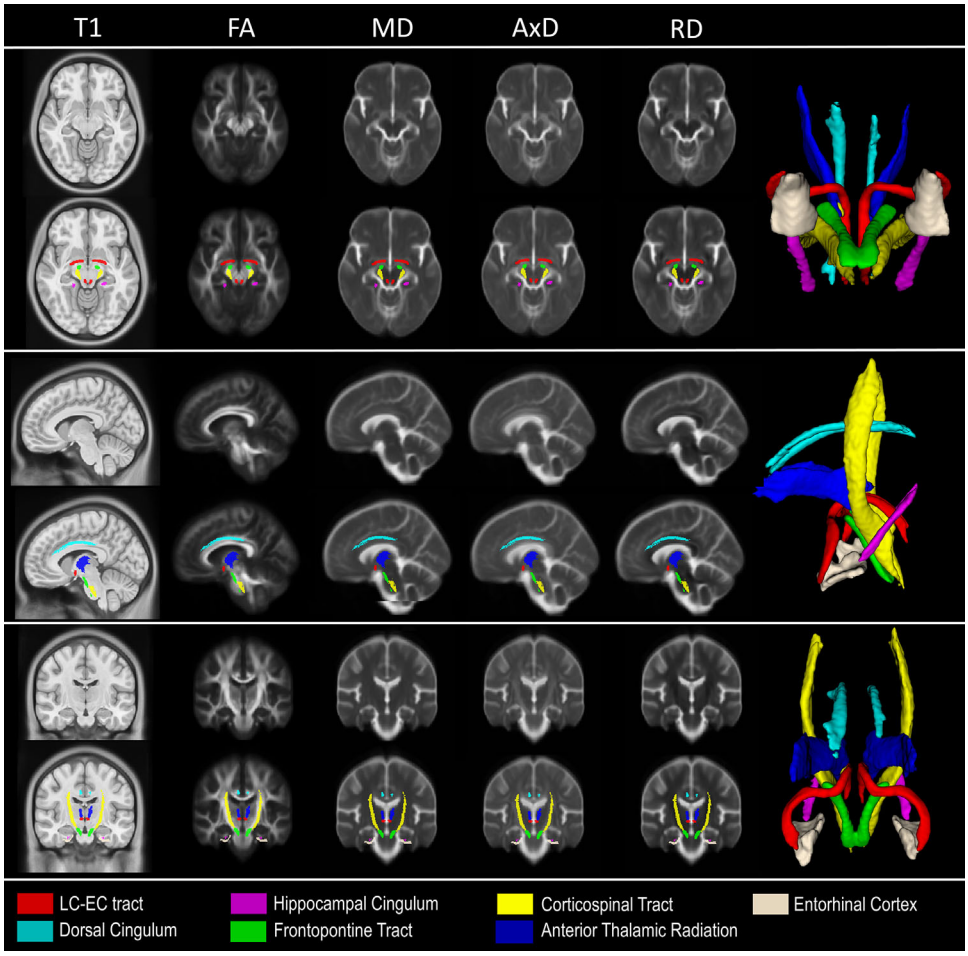

FIGURE 1 Regions of interest were investigated in the study. Each column represents, from left to right: T1 template (MNI152NLin2009cAsym), FA, MD, AxD, and RD maps obtained by averaging all the spatially normalized images. From top to bottom: axial, coronal, and sagittal views; each modality is presented without and with white matter tracts and gray matter regions overlay. Rightmost column: three views of ROIs 3D rendering. Each ROI is represented with a different color (red: locus coeruleus to transentorhinal cortex pathway [LC–EC]; light blue: dorsal subdivisions of the cingulum; fuchsia: hippocampal subdivisions of the cingulum; dark blue: anterior thalamic radiation; yellow: corticospinal tract; green: frontopontine tract; dark white: EC). AxD, axial diffusivity; EC, entorhinal cortex; FA, fractional anisotropy; LC, locus coeruleus; MD, mean diffusivity; MNI, Montreal Neurologic Institute; RD, radial diffusivity; ROI, region of interest.

structural images. For subsequent analyses, the left and right hemispheres were averaged to obtain a single measurement of HV and EC thickness. HVs were normalized by FreeSurfer's estimated total intracranial volume (eTIV). Figure 1 shows, together with tracts of interest, the EC ROI in MNI space.

2.5 | Amyloid PET data acquisition and preprocessing

PET scanning was performed at the nuclear medicine and molecular imaging division at Geneva University Hospitals using a Siemens Biograph mCT or Vision PET scanner (Siemens Healthineers). Amyloid beta images were acquired using 18F-florbetapir (n = 57) or 18F-flutemetamol (n = 67) tracers. 18F-florbetapir images were acquired 50 minutes after the intravenous administration of 200 MBq of the radiotracer (3 × 5-minute image frames). For 18F-flutemetamol, the injected radiotracer's dose was 150 MBq, and images were acquired 90 minutes after the time of injection (4 × 5-minute image frames). Amyloid PET scans were processed using an in-house standard workflow, as described previously.[38] Briefly, amyloid PET images were registered to MNI space via the subject's 3D T1 MRI image. Statistical Parametric Mapping (SPM)12 (Wellcome Trust Centre for Neuroimaging) was used to (1) align PET images to the corresponding T1 MRI image and (2) normalize the T1 images to MNI space using unified segmentation. Standardized uptake value ratio (SUVR) values were generated using the whole cerebellum as a reference region, and data were converted into the Centiloid scale using the region provided by the Global Alzheimer's Association Interactive Network guidelines, which include broader frontal, temporal, parietal, and precuneus cortices and smaller anterior striatal and insular areas.[39] The use of the Centiloid scale ensures that data from the different radiotracers could be compared, and global Centiloid values were used in this study.

2.6 | Tau PET data acquisition and preprocessing

18F-flortaucipir (18F-AV1451), synthesized at the Center for Radiopharmaceutical Sciences ETH-PSI-USZ in Zurich, Switzerland, under license from the intellectual property owner (Avid/Lilly), was used for the tau PET scans. Participants received 180 MBq of 18F-flortaucipir, with image acquisition performed 75 minutes after injection (acquisition time 30 minutes).[40] Each emission frame was reconstructed in 6 × 5-minute frames using a 3D ordered subset expectation maximization iterative reconstruction (4 iterations, 12 subsets), corrected for randoms, dead time, normalization, scatter, attenuation, and sensitivity, and averaged after motion correction. Tau uptake was quantified on PET scans in two composite ROIs defined on FreeSurfer and normalized using the cerebellum as a reference region, based on Braak neuropathological staging: an EC region (corresponding to early tau pathology) and a temporal meta-ROI including the EC, amygdala, fusiform gyrus, inferior temporal gyrus, and middle temporal gyrus (corresponding to more advanced tau pathology).[41]

2.7 | Definition of ATN status

Amyloid PET scans were rated as positive/negative (A+/A−) by a board-certified specialist in nuclear medicine (V.G.) using visual assessment and European Medicines Agency guidelines.[42,43]

Tau positivity/negativity (T+/T−) was defined based on tau PET scans and Braak neuropathological staging[44] by a board-certified specialist in nuclear medicine (V.G.) using visual assessment and published recommendations.[40,45] Participants were classified as T+ according to two classification schemes based on the presence of (1) early or (2) advanced tau pathology. For the early tau classification scheme, participants were classified as T+ if they were in Braak stage I or higher (T_{EC}+). For the advanced tau classification scheme, participants were classified as T+ if they were in Braak stage IV or higher (T_{NEO}+).

Neurodegeneration positivity/negativity (N+/N−) was defined on structural MRI scans using the medial temporal lobe (MTL) atrophy scale,[46] as in previous studies.[47] Visual scores were determined for the left and right hemispheres and averaged. MTL positivity was defined using published age-specific cutoffs (i.e., for participants < 65 years, MTL cut-off ≥ 1; for participants aged 65 to 75 years, MTL cut-off ≥ 1.5; for participants > 75 years, MTL cut-off ≥ 2).[48]

2.8 | Statistical analysis

Statistical analyses were performed using MATLAB version r2018a (Mathworks) and the R package (version 4.2.2). Descriptive statistics reporting mean ± standard deviation values were used for continuous variables. To analyze the relationship between the continuous variables, the Pearson correlation coefficient *r* was calculated, with the related *p* value, for each combination of parameters.

Differences between CU and CI participants in demographic and clinical variables were assessed by one-way analysis of variance (*aov* function) for continuous variables (i.e., age, MMSE) and by χ^2 test for categorical variables (i.e., sex, education level, A+, T_{NEO}+, T_{EC}+, N+).

Differences in microstructural parameters according to cognitive status (CI vs. CU), and biomarker status (A+ vs. A−, T_{NEO}+ vs. T_{NEO}−, T_{EC}+ vs. T_{EC}−, and N+ vs. N−) were assessed with linear regression models (*lm* function) adjusting for age, sex, and education level. Cohen *d* was calculated to evaluate the differences of DWI parametric maps between participants according to cognitive, A, T_{NEO}, T_{EC}, and N status (*cohen.d* function). For all the statistical tests, a *p* value of < 0.05 corrected for multiple comparisons with a false discovery rate (FDR) across 20 tests (i.e., $n = 4$ diffusion indices [FA, MD, RD, AxD] × $n = 5$ status variables [A, T_{NEO}, T_{EC}, N, and cognition]) was considered significant.

To test if these relationships differed between the LC–EC pathway and control tracts, for each significant *lm* model, we tested the interaction between each status variable and the tract variable. For each model, status, tracts, and their interaction were included as independent variables; microstructural measures as the dependent variable, and age, sex, and education as covariates. Two separate sets of models were built, one including only positive control tracts (parahippocampal cingulum and dorsal cingulum) and one including only negative control tracts (anterior thalamic radiation, corticospinal tract, and frontopontine tract).

To investigate potential relationships between the microstructural characteristics of the LC–EC tract and the spatial distribution of tau and amyloid PET tracers, voxel-wise multiple regression analyses were conducted. After spatial normalization, the SUVR PET images underwent an 8-mm Gaussian smoothing. Multiple regression analyses were then performed for each microstructural parameter using SPM12.

To further explore the relationship between LC–EC microstructure and the ATN markers, we also carried out correlations using continuous biomarker measures. This analysis enabled us to assess whether results were consistent across different definitions of biomarkers and to expand our investigation to specific regions such as the EC, which is not incorporated into ATN staging but is relevant to our investigation as it is a major cortical efferent of the LC. To this aim, continuous measures of global amyloid pathology (Centiloid), tau pathology (SUVR in the EC and in the temporal meta-ROI), and neurodegeneration (EC thickness and HV) were extracted. Associations of WM microstructural indices with these ATN markers were assessed with a Pearson correlation test in the whole sample and within cognitive subgroups (i.e., CU and CI). Correlations were corrected for multiple comparisons across 20 tests (i.e., $n = 4$ diffusion indices [FA, MD, RD, AxD] x $n = 5$ biomarkers [Centiloid, tau SUVR in the temporal meta-ROI, tau SUVR in the EC, EC thickness, and HV]) with FDR. A corrected *p* value of < 0.05 was considered significant.

2.9 | Data availability

Anonymized data not published within this article can be made available after a request from any qualified investigator.

3 | RESULTS

3.1 | Demographic, clinical, and biomarker features

Table 1 shows the demographic, cognitive, and ATN features of participants. Statistical comparisons showed that A and T biomarkers discriminated CI from CU ($p < 0.001$), while N showed a trend for significance ($p = 0.075$). Figure S1 in supporting information shows the average amyloid and tau PET uptake in the CI and CU groups.

On cognitive and ATN classification, the majority of CI participants were at the MCI stage (85%) and in the AD continuum (A+: 73%), while the remaining participants either showed a negative biomarker profile (A–T–N–: 16%) or non-AD pathologic changes (A–, positive for either N or T: 11%). The majority of CU participants showed a negative biomarker profile (A–T–N–: 67%), while 10 participants were positive to at least one ATN biomarker: 23% were in the AD continuum (A+), and 10% were characterized by non-AD pathological changes (A–T–N+).

3.2 | LC-EC microstructural measures are associated with positivity to T and N markers and cognitive impairment

Table 2 and Figure S2 in supporting information report the results of the differences in the diffusion measures of the LC–EC tract according to ATN markers and cognition.

No differences were detected between A+ and A– participants ($p \geq 0.153$) nor between T_{NEO}+ and T_{NEO}– participants (i.e., Braak ≥ IV stage, $p \geq 0.045$, not surviving multiple comparisons correction). Differences in diffusion measures of the LC–EC tract were detected when participants were classified according to positivity for early tau (T_{EC}+ vs. T_{EC}–) and positivity to neurodegeneration (N+ vs. N–). Specifically, T_{EC}+ participants showed lower FA ($d = 0.48$; $p = 0.020$), higher MD ($d = -0.60$; $p = 0.002$), and higher RD ($d = -0.63$; $p = 0.001$) and AxD ($d = -0.55$; $p = 0.004$) than T_{EC}–. N+ showed higher MD ($d = -0.86$; $p < 0.001$), RD ($d = -0.86$; $p < 0.001$), and AxD ($d = -0.85$; $p < 0.001$) compared to N–, while FA was not significant (Table 2; Figure S2).

When considering cognitive status, higher MD ($d = -0.59$; $p = 0.009$), RD ($d = -0.61$; $p = 0.007$), and AxD ($d = -0.54$; $p = 0.019$) were detected in CI patients compared to CU, while differences in FA were not significant (Table 2).

Figure S3 in supporting information shows the trend of the microstructural measures along the LC–EC tract. The assessment of microstructural differences along the entire tract showed higher diffusivity in CI versus CU participants in the rostral part of the tract, especially in MD and RD measures ($p < 0.05$, cluster-based permutation tests). Conversely, the caudal portion of the LC tract showed lower FA and lower AxD in CI compared to CU participants ($p < 0.05$, cluster-based permutation tests), suggesting that distinct neurodegenerative processes may affect the rostral and caudal segments of the LC pathway. The voxel-wise multiple regression analyses of tau PET and amyloid PET signals did not identify any brain regions exhibiting statistically significant correlations ($p < 0.05$, family-wise error corrected) with the microstructural markers of LC–EC. These findings suggest no discernible relationship between LC–EC microstructural parameters and the cortical distribution patterns of the two radiotracers.

3.3 | Analysis in control tracts

In terms of positive control tracts, the parahippocampal and dorsal cingulum control tracts showed significant and robust differences according to neurodegeneration: N+ participants showing higher MD, RD, AxD, and lower FA than N– ($0.58 < |d| < 1.08$; $p < 0.05$ after FDR correction; Tables S1 and S2 in supporting information). These differences were comparable to those observed in the LC–EC tract, except for FA, which showed more pronounced effects in the dorsal cingulum versus the LC–EC tract ($p < 0.001$; Figure S4 in supporting information), and MD and AxD, which were higher in the LC–EC versus the dorsal cingulum tract ($p < 0.05$; Figure S4). For the comparison between T_{EC}+ and T_{EC}–, the former group showed significantly higher MD, RD, and AxD in the parahippocampal tract ($0.64 < |d| < 0.72$; Table S1), which was comparable to the LC–EC tract (interaction term: $p > 0.05$). The dorsal cingulum tract showed no difference for the comparison between T_{EC}+ and T_{EC}– (Table S2), and the interaction analysis confirmed that these differences were more pronounced in the LC–EC tract (MD and AxD: $p < 0.05$; Figure S4). While the positive control tracts showed no difference in DWI metrics according to cognitive status (CI vs. CU; $p > 0.05$ after FDR correction; Tables S1 and S2), the interaction term with the LC–EC tract was not significant ($p > 0.05$), indicating a comparable degree of impairment. Similarly to the LC–EC pathway, no difference was detected in the positive control tracts according to amyloid (A+ vs. A–) or advanced tau pathology (T_{NEO}: Braak IV–VI vs. Braak 0–III), except for higher AxD in the parahippocampal tract in T_{NEO}+ versus T_{NEO}– ($p = 0.010$; all other $p > 0.05$ after FDR correction; Tables S1 and S2), with no significant interaction effects (all $p > 0.05$).

In negative control tracts, as expected, microstructural measures of tracts affected at later stages in AD, such as the anterior thalamic radiation, corticospinal, and frontopontine tracts, were weakly associated with ATN pathology and cognition. Specifically, no difference was observed in these tracts according to amyloid, tau (both early and advanced pathology), and cognitive status (Tables S3–S5 in supporting information). A significant difference was observed only for the comparison between N+ and N– in the anterior thalamic radiation (i.e., higher MD, RD, and AxD in the N+ group; $1.03 < |d| < 1.06$) and corticospinal tract (higher AxD in the N+ group, $d = 0.58$; Table S4). The interaction analysis confirmed that microstructural differences were more pronounced in the LC–EC tract than in the negative control tracts for the comparisons T_{EC}+ versus T_{EC}– (significant interaction with corticospinal tract) and N+ versus N– (significant interaction with corticospinal and frontopontine tracts; Figure S5 in supporting information).

TABLE 2 Microstructural alterations in the LC–EC tract according to ATN and cognitive status.

Amyloid	A– *N* = 48	A+ *N* = 76	*d*	*p*
FA	0.313 ± 0.016	0.310 ± 0.018	0.177	0.373
MD (μm²/s)	1.105 ± 0.099	1.141 ± 0.102	−0.355	0.157
RD (μm²/s)	0.934 ± 0.092	0.968 ± 0.097	−0.356	0.153
AxD (μm²/s)	1.448 ± 0.115	1.488 ± 0.114	−0.346	0.174
Tau_{EC}	**T– (Braak 0)** ***N* = 53**	**T+ (Braak I–VI)** ***N* = 71**	***d***	***p***
FA	0.316 ± 0.017	0.308 ± 0.016	0.479	**0.020***
MD	1.093 ± 0.101	1.153 ± 0.095	−0.604	**0.002***
RD	0.921 ± 0.095	0.980 ± 0.090	−0.627	**0.001***
AxD	1.437 ± 0.115	1.499 ± 0.109	−0.553	**0.004***
Tau_{NEO}	**T– (Braak 0–III)** ***N* = 73**	**T+ (Braak IV–VI)** ***N* = 51**	***d***	***p***
FA	0.314 ± 0.018	0.309 ± 0.015	0.288	0.196
MD	1.117 ± 0.111	1.142 ± 0.087	−0.242	0.045
RD	0.945 ± 0.105	0.969 ± 0.082	−0.253	0.046
AxD	1.462 ± 0.126	1.488 ± 0.098	−0.219	0.049
Neurodegeneration	**N–** ***N* = 89**	**N+** ***N* = 34**	***d***	***p***
FA	0.313 ± 0.015	0.309 ± 0.020	0.221	0.344
MD	1.103 ± 0.092	1.185 ± 0.102	−0.859	**< 0.001***
RD	0.932 ± 0.086	1.009 ± 0.099	−0.857	**< 0.001***
AxD	1.446 ± 0.107	1.538 ± 0.111	−0.845	**< 0.001***
Cognition	**CU** ***N* = 30**	**CI** ***N* = 94**	***d***	***p***
FA	0.317 ± 0.017	0.310 ± 0.017	0.395	0.052
MD	1.083 ± 0.094	1.142 ± 0.101	−0.589	**0.009***
RD	0.911 ± 0.088	0.969 ± 0.095	−0.613	**0.007***
AxD	1.426 ± 0.109	1.487 ± 0.114	−0.537	**0.019***

Note: Values denote mean ± standard deviation. *P* denotes significance on one-way analysis of variance test, adjusted for age, sex, and education level. Asterisks denote *p* value < 0.05 after false discovery rate correction for multiple comparisons.
Abbreviations: A–, amyloid negative; A+, amyloid positive; AxD, axial diffusivity; CI, cognitively impaired; CU, cognitively unimpaired; *d* = Cohen effect size; FA, fractional anisotropy; LC, locus coeruleus; MD, mean diffusivity; N–, medial temporal lobe atrophy negative; N+, medial temporal lobe atrophy positive; RD, radial diffusivity; T–, tau negative; T+, tau positive.

3.4 | LC–EC microstructural measures are associated with EC neurodegeneration

Associations between LC–EC microstructure and continuous measures of ATN markers were assessed with Pearson correlation.

No association was detected between LC–EC diffusivity measures and amyloid uptake (Centiloid) in the whole sample nor in clinical subgroups ($p > 0.05$ after FDR correction; Figure S6 in supporting information).

Lower LC–EC FA correlated with higher tau in the EC ($r = -0.224$; $p = 0.012$) and the temporal meta-ROI ($r = -0.225$; $p = 0.012$) in the whole sample. Both correlations remained significant after FDR correction; however, no significant association was detected in clinical subgroups (all $p > 0.05$; Figures S7 and S8 in supporting information). No association was detected between tau (EC and meta-ROI) and MD, AxD, and RD measures (all $p > 0.05$ FDR corrected; Figures S7 and S8).

Lower LC–EC FA was associated with lower EC thickness in the whole sample ($r = 0.198$; $p = 0.027$) and in CI participants ($r = 0.207$; $p = 0.045$; Figure 2, top left panel), but was not significant after multiple comparisons correction ($p > 0.05$ FDR corrected). Higher LC–EC MD, RD, and AxD were associated with lower EC thickness in the whole sample (Figure 2; all $p < 0.001$, significant after FDR correction) and in CI patients (all $p < 0.001$, significant after FDR correction). A similar pattern of negative correlations was observed between LC–EC diffusion measures (MD, AxD, RD) and HVs in the whole sample (all

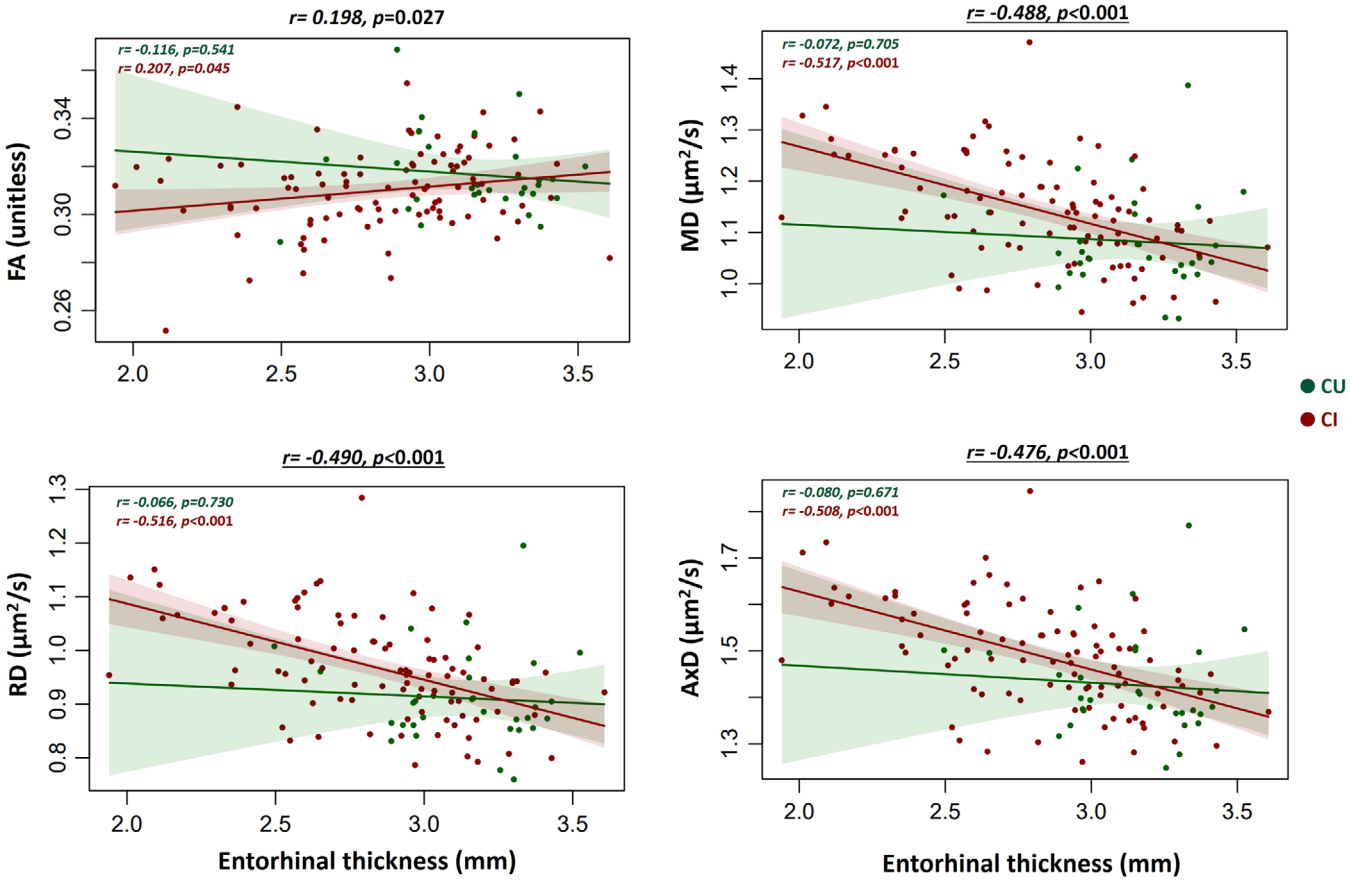

FIGURE 2 Correlations between LC–EC microstructural measures (FA, MD, RD, AxD) and entorhinal cortex thickness. *P* values surviving multiple comparisons correction (FDR) are underlined. AxD, axial diffusivity; EC, entorhinal cortex; FA, fractional anisotropy; FDR, false discovery rate; LC, locus coeruleus; MD, mean diffusivity; RD, radial diffusivity.

$p < 0.001$) and within subgroups (all $p < 0.001$; Figure S9 in supporting information; all significant after FDR correction).

3.5 | LC–EC microstructural measures predict cognitive impairment

The univariate models identified the MD of the LC–EC tract as the microstructural predictor most strongly associated with CI (Table S6 in supporting information). For tau PET measures, temporal meta-ROI uptake was a better predictor than EC uptake, and HV was a better predictor than EC thickness (Table S6). Amyloid PET Centiloid was also significantly associated with the dependent variable.

The results of the linear regression models are presented in Table 3. The model showed that LC–EC MD remained a significant predictor of CI even after accounting for ATN markers ($p = 0.015$). In detail, the multiple linear regression model identified age, education, tau, and LC–EC MD as predictors of MMSE score.

The analysis in the control tracts identified the AxD of the parahippocampus and RD of the dorsal cingulum as the best predictors in the univariate models. Model comparison showed that the dorsal cingulum performed better than the parahippocampus and similarly to the LC–EC tract (Akaike information criterion [AIC]: 683 vs. 689 vs. 683; Bayesian information criterion [BIC]: 700 vs. 706 vs. 700; residual standard error = 3.69 vs. 3.78 vs. 3.69, respectively). Similar results between the LC–EC pathway and dorsal cingulum were obtained when

TABLE 3 Multiple linear regression model evaluating the utility of LC–EC microstructure assessment in predicting MMSE.

Variable	Std. coefficient	*p*	Partial eta-squared
Age (years)	0.31	<0.001	0.07
Sex (females)	−0.13	0.441	0.05
Education (years)	0.28	<0.001	0.18
Amyloid (Centiloid)	−0.06	0.577	0.12
Tau (SUVR temporal meta-ROI)	−0.29	0.012	0.10
HV (mm^3)	0.07	0.437	0.04
LC to EC tract MD ($\mu m^2/s$)	−0.22	0.015	0.05

Abbreviations: EC, entorhinal cortex; HV, hippocampal volume; LC, locus coeruleus; MD, mean diffusivity; MMSE, Mini-Mental State Examination; ROI, region of interest; SUVR, standardized uptake value ratio.

measures of ATN were included in the multivariate model (AIC: 663 vs. 660; BIC: 688 vs. 685; residual standard error = 3.44 vs. 3.40).

4 | DISCUSSION

This study provides a comprehensive assessment of LC–EC pathway microstructure in relation to ATN biomarkers and cognition in memory clinic patients. We reported that: (1) LC–EC diffusion metrics were associated with tau and neurodegeneration in the MTL and with cognition; (2) LC–EC MD significantly predicted CI even after accounting for ATN markers; (3) LC–EC diffusion measures were as sensitive as cingular tracts in detecting CI but showed higher sensitivity in detecting MTL tau pathology and neurodegeneration.

4.1 | Relationship between LC–EC microstructure and CI

Our results extend previous reports showing that LC-EC microstructural measures are sensitive to CI.[13–15] Specifically, we confirmed that increased RD in the LC–EC pathway can be detected in patients with CI,[13,14] and we reported for the first time increased MD and AxD in these patients, as previous studies either did not assess these metrics[13,15] or reported no difference.[14] Overall, these results indicate that diffusivity measures (MD, AxD, RD) are sensitive to LC–EC alterations and that RD best differentiates between CI and CU based on Cohen *d* effect sizes (Table 2). Contrary to our hypothesis, we did not detect significant differences in FA; however, we note that this negative result is consistent with a previous study that assessed this metric,[15] and with previous observations that FA may be less sensitive than diffusivity measures in AD.[10,49] Comparisons to tracts typically affected in dementia showed that the LC–EC pathway was as sensitive as the parahippocampal and cingulum tracts in detecting CI, as indicated by the regression models and the interaction analysis, although we note that only LC–EC tract diffusivity could discriminate CI from CU participants (Table 2).

4.2 | Relationship between LC–EC microstructure and ATN markers

The mechanism linking the LC–EC tract microstructure to AD pathophysiology remains largely unclear. Based on the revised Braak staging model and previous studies,[3,6,8,22,23,50] we hypothesized that the LC–EC tract microstructure would be primarily related to tau (T) in the EC and neocortex and to neurodegeneration (N) markers. Our results partially confirm this prediction as we observed that LC–EC microstructure was associated with positivity to tau pathology in both EC and neocortical areas (i.e., Braak stage ≥ I) and to neurodegeneration, but not to more advanced tau pathology (i.e., Braak stage ≥ IV), in contrast with previous LC-MRI studies reporting an association between LC impairment and higher Braak stages.[3,6,22] A possible explanation for these discrepancies may relate to the different imaging metrics used in these studies (i.e., DWI vs. LC-MRI). We speculate that DTI metrics might be more sensitive to early tau processes in the EC, while LC-MRI may be sensitive to both early and advanced tau-related processes. Finally, we note that the lack of associations with amyloid pathology is in line with previous neuropathological and LC-MRI studies,[24,25] and confirms that LC-related alterations are independent of amyloid pathology. The analysis on dichotomous (Table 2) and continuous measures (Figure 2 and Figures S6–S9) provided both consistent and complementary information. Specifically, the analyses on continuous measures confirmed the null results about amyloid and advanced tau pathology and the positive results on MTL atrophy. Moreover, while LC–EC microstructural measures were sensitive to tau pathology in Braak stages I through VI, no association was detected with continuous measures of local tau pathology, including average SUVR in the EC and meta-ROI and whole-brain voxel-wise analysis, indicating that diffusivity measures are sensitive to the presence of tau pathology regardless of its regional distribution.

Notably, LC–EC microstructural features showed stronger associations with MTL neurodegeneration than with EC tau pathology. Cohen effect sizes were indeed large for N (0.84–0.86) and medium for T_{EC}+ (0.55–0.63); moreover, LC–EC diffusion measures showed robust correlations with EC and HV (Figure 2, Figure S9), while no association was detected with tau in the EC and meta-ROI (Figures S7 and S8). This finding partially agrees with our previous study in an independent sample showing that LC–EC tract microstructure is associated with EC atrophy in patients with dementia.[14] The stronger association of LC–EC microstructure with MTL neurodegeneration than with EC tau suggests that LC–EC abnormalities are secondary to MTL neurodegeneration.[14] Axons arising from the LC are densely packed and extensively project to MTL regions. Axonal loss/degeneration secondary to MTL atrophy may increase axonal membrane permeability and reduce extra-axonal space, thereby increasing RD, AxD, and MD. FA measures, which reflect the ratio of AxD to RD, may be less sensitive to axonal changes when there is a concurrent increase in the two directional measures. Another possible explanation may be that LC–EC neurodegeneration is secondary to LC damage, but we cannot directly answer this question because we did not assess LC integrity using LC-MRI. This hypothesis is supported by neuropathological studies showing that noradrenergic axon damage may be present due to tau cytoskeletal pathology and dendritic atrophy in tangle-bearing LC neurons in Braak stages 0 and I,[7,9] while LC cellular loss starts later (Braak stages III–IV).[6] Finally, another possible mechanism may involve degeneration of other subcortical regions connected to the LC–EC tract, such as the thalamus and the nucleus basalis of Meynert.[51] The analysis in control tracts showed that the parahippocampal diffusivity pattern was comparable to that of the LC–EC pathway, being significantly associated with T_{EC}+ and N+ markers. As expected, tracts affected later in AD (i.e., dorsal cingulum, anterior thalamic radiation, frontopontine, corticospinal) showed no association with T_{EC}+ and T_{NEO}+, and the interaction analysis confirmed the more pronounced effect in the LC–EC tract for the comparison between T_{EC}+ and T_{EC}−. For N+ status, a divergent pattern was observed between the LC–EC pathway and

the dorsal cingulum, whereby MD/AxD measures were more affected in the former and FA in the latter, suggesting distinct pathological mechanisms. The anterior thalamic tract showed a pattern of neurodegeneration comparable to the LC–EC tract, which was unexpected given our hypothesis of a relative preservation of this tract. This result may be explained by the extensive projections of this pathway to the thalamus and recent observations that it may contribute to the Papez circuit equally to the parahippocampus.[52]

4.3 | Clinical value of LC–EC microstructural alterations in predicting cognitive impairment

When we tested whether LC–EC measures predicted CI after controlling for ATN markers, we found that MD was still significantly associated with cognition. While the factor contributing most strongly in the model was tau, LC–EC MD was still marginally significant, supporting the added value of LC–EC diffusivity in predicting CI. The EC and hippocampus are brain regions receiving major pathways originating from the LC. These regions regulate memory formation and consolidation and are affected early in AD dementia. The relevance of these LC pathways to cognition is supported by previous studies in normal aging and dementia showing associations between memory performance and LC microstructure.[15,53] The analysis in the control tracts showed that the performance of the LC–EC tract was comparable to that of the dorsal cingulum and parahippocampal tract. Our results confirm and extend this literature, showing that LC–EC structural connectivity can contribute to cognitive deficits. In addition, these results corroborate previous evidence that cognitive decline is more associated with downstream pathological processes instead of amyloidosis.[54–56]

4.4 | Limitations and strengths

This study has some limitations. First, this work lacks a direct assessment of the LC region with ad hoc MRI sequences such as LC-MRI.[24,57–61] The assessment of the LC region with LC-MRI will be important to confirm previous studies demonstrating that LC volume loss or reduced integrity is associated with LC fiber loss, higher Braak stage, and progression of dementia,[3,6,22,23,50] and to better inform on the mechanism underlying microstructural impairment, that is, whether it is secondary to degeneration rather than to the afferent or efferent region (i.e., LC vs. EC). In addition, the MR diffusion protocol used in our study did not enable the performance of tractography analysis,[62] as it included just one b-shell and did not allow the use of specific techniques to control for CSF contamination, such as free water elimination.[63,64] However, the use of tractography to reconstruct the LC–EC pathway is challenging due to the lack of ground truth in humans and the complex orientation of fibers branching off to the EC, which can produce multiple plausible routes.[21] Our choice of an atlas-based approach for LC–EC segmentation presents advantages such as groupwise consistency and ease of use in clinical settings, where advanced DWI protocols may not be available. Still, atlas-based approaches have limitations in terms of generalizability and accuracy in registration, which require careful inspection of individual outputs. Finally, future studies with larger samples are needed to investigate the contribution of other non-AD pathologies (e.g., primary age-related tauopathy and suspected non-AD pathophysiology), and longitudinal cognitive data will be important to further evaluate the value of LC–EC microstructure in predicting cognitive decline.

A strength of the study is the well-characterized cohort with ATN markers, which enabled us to comprehensively investigate the relationship between microstructural LC–EC features and AD markers compared to previous studies in CI cohorts.[14,15] Another advantage is that the results were obtained from observational neuroimaging data collected in clinical practice, thereby supporting the clinical translation of the methodology.

5 | CONCLUSIONS

Our results show that the study of LC–EC microstructure can improve our understanding of the mechanisms underlying CI and provide new potential clinical markers for the diagnosis of cognitive decline.

ACKNOWLEDGMENTS

The Clinical Research Center, at Geneva University Hospital and Faculty of Medicine provides valuable support for regulatory submissions and data management, and the Biobank at Geneva University Hospital for biofluid processing and storage. The authors thank Avid Radiopharmaceuticals Inc. for providing the 18F-Flortaucipir tracer without being involved in the data analysis or interpretation. IRCCS SYNLAB SDN is partially supported by #NEXTGENERATIONEU (NGEU) and funded by the Ministry of University and Research (MUR), National Recovery and Resilience Plan (NRRP), project MNESYS (PE0000006) – A Multiscale integrated approach to the study of the nervous system in health and disease (DN. 1553 11.10.2022, CC and MS) and Italian Ministry of Health (project GR-2018-12366779 and RICERCA CORRENTE). The Centre de la mémoire is funded by the following private donors under the supervision of the Private Foundation of Geneva University Hospitals: A.P.R.A.—Association Suisse pour la Recherche sur la Maladie d'Alzheimer, Genève; Fondation Segré, Genève; Race Against Dementia Foundation, London, UK; Fondation Child Care, Genève; Fondation Edmond J. Safra, Genève; Fondation Minkoff, Genève; Fondazione Agusta, Lugano; McCall Macbain Foundation, Canada; Nicole et René Keller, Genève; Fondation AETAS, Genève. Competitive research projects have been funded by: H2020 (projects n. 667375), Innovative Medicines Initiative (IMI contract n. 115736 and 115952), IMI2, Swiss National Science Foundation (projects n.320030_182772, 320030_185028, and n. 320030_169876), VELUX Foundation, Schmidheiny foundation. The IRCCS Fatebenefratelli is partially supported by the Italian Ministry of Health (Ricerca Corrente). IOJ is funded by SNSF Eccellenza PCEFP2_194260.

CONFLICT OF INTEREST STATEMENT

The authors report no disclosures relevant to the manuscript. Author disclosures are available in the supporting information.

CONSENT STATEMENT

This study was approved by the local ethics committee and has been conducted in accordance with the principles of the Declaration of Helsinki and the International Conference on Harmonization Good Clinical Practice guidelines. Each participant provided a voluntary written informed consent for retrospective analysis of clinical, biological, and imaging data (PB_2016-01346, 2020-00403).

REFERENCES

1. Poe GR, Foote S, Eschenko O, et al. Locus coeruleus: a new look at the blue spot. *Nat Rev Neurosci*. 2020;21(11):644-659. doi:10.1038/s41583-020-0360-9
2. Bouret S, Sara SJ. Network reset: a simplified overarching theory of locus coeruleus noradrenaline function. *Trends Neurosci*. 2005;28(11):574-582. doi:10.1016/j.tins.2005.09.002
3. Jacobs HIL, Becker JA, Kwong K, et al. In vivo and neuropathology data support locus coeruleus integrity as indicator of Alzheimer's disease pathology and cognitive decline. *Sci Transl Med*. 2021;13(612):eabj2511. doi:10.1126/scitranslmed.abj2511
4. Galgani A, Lombardo F, Martini N, et al. Magnetic resonance imaging locus coeruleus abnormality in amnestic mild cognitive impairment is associated with future progression to dementia. *Eur J Neurol*. 2023;30(1):32-46. doi:10.1111/ene.15556
5. Elman JA, Puckett OK, Beck A, et al. MRI-assessed locus coeruleus integrity is heritable and associated with multiple cognitive domains, mild cognitive impairment, and daytime dysfunction. *Alzheimers Dement*. 2021;17(6):1017-1025. doi:10.1002/alz.12261
6. Theofilas P, Ehrenberg AJ, Dunlop S, et al. Locus coeruleus volume and cell population changes during Alzheimer's disease progression: a stereological study in human postmortem brains with potential implication for early-stage biomarker discovery. *Alzheimers Dement*. 2017;13(3):236-246. doi:10.1016/j.jalz.2016.06.2362
7. Weinshenker D. Long road to ruin: noradrenergic dysfunction in neurodegenerative disease. *Trends Neurosci*. 2018;41(4):211-223. doi:10.1016/j.tins.2018.01.010
8. Braak H, Thal DR, Ghebremedhin E, Del Tredici K. Stages of the pathologic process in Alzheimer disease: age categories from 1 to 100 years. *J Neuropathol Exp Neurol*. 2011;70(11):960-969. doi:10.1097/NEN.0b013e318232a379
9. Gilvesy A, Husen E, Magloczky Z, et al. Spatiotemporal characterization of cellular tau pathology in the human locus coeruleus–pericoerulear complex by three-dimensional imaging. *Acta Neuropathol*. 2022;144(4):651-676. doi:10.1007/s00401-022-02477-6
10. Acosta-Cabronero J, Nestor PJ. Diffusion tensor imaging in Alzheimer's disease: insights into the limbic-diencephalic network and methodological considerations. *Front Aging Neurosci*. 2014;6:266. Accessed April 17, 2023 https://www.frontiersin.org/articles/10.3389/fnagi.2014.00266
11. Clerx L, Visser PJ, Verhey F, Aalten P. New MRI markers for Alzheimer's disease: a meta-analysis of diffusion tensor imaging and a comparison with medial temporal lobe measurements. *J Alzheimers Dis*. 2012;29(2):405-429. doi:10.3233/JAD-2011-110797
12. Sexton CE, Kalu UG, Filippini N, Mackay CE, Ebmeier KP. A meta-analysis of diffusion tensor imaging in mild cognitive impairment and Alzheimer's disease. *Neurobiol Aging*. 2011;32(12):2322.e5-18. doi:10.1016/j.neurobiolaging.2010.05.019
13. Sun W, Tang Y, Qiao Y, et al. A probabilistic atlas of locus coeruleus pathways to transentorhinal cortex for connectome imaging in Alzheimer's disease. *NeuroImage*. 2020;223:117301. doi:10.1016/j.neuroimage.2020.117301
14. Quattrini G, Pini L, Boscolo Galazzo I, et al. Microstructural alterations in the locus coeruleus-entorhinal cortex pathway in Alzheimer's disease and frontotemporal dementia. *Alzheimers Dement*. 2024;16(1):e12513. doi:10.1002/dad2.12513
15. Chu WT, Wang WE, Zaborszky L, et al. Association of cognitive impairment with free water in the nucleus basalis of Meynert and locus coeruleus to transentorhinal cortex tract. *Neurology*. 2022;98(7):e700-e710. doi:10.1212/WNL.0000000000013206
16. Porat S, Sibilia F, Yoon J, et al. Age differences in diffusivity in the locus coeruleus and its ascending noradrenergic tract. *NeuroImage*. 2022;251:119022. doi:10.1016/j.neuroimage.2022.119022
17. Langley J, Hussain S, Huddleston DE, Bennett IJ, Hu XP. Impact of locus coeruleus and its projections on memory and aging. *Brain Connect*. 2022;12(3):223-233. doi:10.1089/brain.2020.0947
18. Irwin DJ, Brettschneider J, McMillan CT, et al. Deep clinical and neuropathological phenotyping of Pick disease. *Ann Neurol*. 2016;79(2):272-287. doi:10.1002/ana.24559
19. Brunnström H, Friberg N, Lindberg E, Englund E. Differential degeneration of the locus coeruleus in dementia subtypes. *Clin Neuropathol*. 2011;30(3):104-110. doi:10.5414/npp30104
20. Haglund M, Friberg N, Danielsson EJD, Norrman J, Englund E. A methodological study of locus coeruleus degeneration in dementing disorders. *Clin Neuropathol*. 2016;35(5):287-294. doi:10.5414/NP300930
21. Solders SK, Galinsky VL, Clark AL, et al. Diffusion MRI tractography of the locus coeruleus-transentorhinal cortex connections using GO-ESP. *Magn Reson Med*. 2022;87(4):1816-1831. doi:10.1002/mrm.29088
22. Cassidy CM, Therriault J, Pascoal TA, et al. Association of locus coeruleus integrity with Braak stage and neuropsychiatric symptom severity in Alzheimer's disease. *Neuropsychopharmacol*. 2022;47(5):1128-1136. doi:10.1038/s41386-022-01293-6
23. Kelly SC, He B, Perez SE, Ginsberg SD, Mufson EJ, Counts SE. Locus coeruleus cellular and molecular pathology during the progression of Alzheimer's disease. *Acta Neuropathol Commun*. 2017;5(1):8. doi:10.1186/s40478-017-0411-2
24. Olivieri P, Lagarde J, Lehericy S, et al. Early alteration of the locus coeruleus in phenotypic variants of Alzheimer's disease. *Ann Clin Transl Neurol*. 2019;6(7):1345-1351. doi:10.1002/acn3.50818
25. Murray ME, Moloney CM, Kouri N, et al. Global neuropathologic severity of Alzheimer's disease and locus coeruleus vulnerability influences plasma phosphorylated tau levels. *Mol Neurodegener*. 2022;17(1):85. doi:10.1186/s13024-022-00578-0
26. von Elm E, Altman DG, Egger M, Pocock SJ, Gøtzsche PC, Vandenbroucke JP. Strengthening the Reporting of Observational Studies in Epidemiology (STROBE) statement: guidelines for reporting observational studies. *BMJ*. 2007;335(7624):806-808. doi:10.1136/bmj.39335.541782.AD
27. Ribaldi F, Chicherio C, Altomare D, et al. Brain connectivity and metacognition in persons with subjective cognitive decline (COSCODE): rationale and study design. *Alzheimers Res Ther*. 2021;13(1):105. doi:10.1186/s13195-021-00846-z
28. Albert MS, DeKosky ST, Dickson D, et al. The diagnosis of mild cognitive impairment due to Alzheimer's disease: recommendations from the National Institute on Aging-Alzheimer's Association workgroups on diagnostic guidelines for Alzheimer's disease. *Alzheimers Dement*. 2011;7(3):270-279. doi:10.1016/j.jalz.2011.03.008
29. McKhann GM, Knopman DS, Chertkow H, et al. The diagnosis of dementia due to Alzheimer's disease: recommendations from the

National Institute on Aging-Alzheimer's Association workgroups on diagnostic guidelines for Alzheimer's disease. *Alzheimers Dement*. 2011;7(3):263-269. doi:10.1016/j.jalz.2011.03.005

30. Veraart J, Novikov DS, Christiaens D, Ades-aron B, Sijbers J, Fieremans E. Denoising of diffusion MRI using random matrix theory. *NeuroImage*. 2016;142:394-406. doi:10.1016/j.neuroimage.2016.08.016
31. Andersson JLR, Sotiropoulos SN. Non-parametric representation and prediction of single- and multi-shell diffusion-weighted MRI data using Gaussian processes. *NeuroImage*. 2015;122:166-176. doi:10.1016/j.neuroimage.2015.07.067
32. Tournier JD, Smith R, Raffelt D, et al. MRtrix3: a fast, flexible and open software framework for medical image processing and visualisation. *NeuroImage*. 2019;202:116137. doi:10.1016/j.neuroimage.2019.116137
33. Jenkinson M, Beckmann CF, Behrens TEJ, Woolrich MW, Smith SM. FSL. *NeuroImage*. 2012;62(2):782-790. doi:10.1016/j.neuroimage.2011.09.015
34. Catani M. Diffusion tensor magnetic resonance imaging tractography in cognitive disorders. *Curr Opin Neurol*. 2006;19(6):599-606. doi:10.1097/01.wco.0000247610.44106.3f
35. Zhang Y, Brady M, Smith S. Segmentation of brain MR images through a hidden Markov random field model and the expectation-maximization algorithm. *IEEE Trans Med Imaging*. 2001;20(1):45-57. doi:10.1109/42.906424
36. Tang Y, Sun W, Toga AW, Ringman JM, Shi Y. A probabilistic atlas of human brainstem pathways based on connectome imaging data. *NeuroImage*. 2018;169:227-239. doi:10.1016/j.neuroimage.2017.12.042
37. Dale AM, Fischl B, Sereno MI. Cortical surface-based analysis: I. segmentation and surface reconstruction. *NeuroImage*. 1999;9(2):179-194. doi:10.1006/nimg.1998.0395
38. Peretti DE, Ribaldi F, Scheffler M, Chicherio C, Frisoni GB, Garibotto V. Prognostic value of imaging-based ATN profiles in a memory clinic cohort. *Eur J Nucl Med Mol Imaging*. 2023;50(11):3313-3323. doi:10.1007/s00259-023-06311-3
39. Klunk WE, Koeppe RA, Price JC, et al. The Centiloid Project: standardizing quantitative amyloid plaque estimation by PET. *Alzheimers Dement*. 2015;11(1):1-15 .e1-4. doi:10.1016/j.jalz.2014.07.003
40. Mathoux G, Boccalini C, Peretti DE, et al. A comparison of visual assessment and semi-quantification for the diagnostic and prognostic use of [18F]flortaucipir PET in a memory clinic cohort. *Eur J Nucl Med Mol Imaging*. 2024;51(6):1639-1650. Published online January 6, 2024. doi:10.1007/s00259-023-06583-9
41. Jack CR, Wiste HJ, Weigand SD, et al. Defining imaging biomarker cut-points for brain aging and Alzheimer's disease. *Alzheimers Dement*. 2017;13(3):205-216. doi:10.1016/j.jalz.2016.08.005
42. European Medicines Agency. https://www.ema.europa.eu/en/medicines/human/EPAR/amyvid
43. European Medicines Agency. https://www.ema.europa.eu/en/medicines/human/EPAR/vizamyl
44. Braak H, Alafuzoff I, Arzberger T, Kretzschmar H, Del Tredici K. Staging of Alzheimer disease-associated neurofibrillary pathology using paraffin sections and immunocytochemistry. *Acta Neuropathol*. 2006;112(4):389-404. doi:10.1007/s00401-006-0127-z
45. Fleisher AS, Pontecorvo MJ, Devous MD Sr, et al. Positron emission tomography imaging with [18F]flortaucipir and postmortem assessment of Alzheimer disease neuropathologic changes. *JAMA Neurol*. 2020;77(7):829-839. doi:10.1001/jamaneurol.2020.0528
46. Scheltens P, Leys D, Barkhof F, et al. Atrophy of medial temporal lobes on MRI in "probable" Alzheimer's disease and normal ageing: diagnostic value and neuropsychological correlates. *J Neurol Neurosurg Psychiatry*. 1992;55(10):967-972. doi:10.1136/jnnp.55.10.967
47. Altomare D, Stampacchia S, Ribaldi F, et al. Plasma biomarkers for Alzheimer's disease: a field-test in a memory clinic. *J Neurol Neurosurg Psychiatry*. 2023;94(6):420-427. doi:10.1136/jnnp-2022-330619
48. Rhodius-Meester HFM, Benedictus MR, Wattjes MP, et al. MRI visual ratings of brain atrophy and white matter hyperintensities across the spectrum of cognitive decline are differently affected by age and diagnosis. *Front Aging Neurosci*. 2017;9:117. doi:10.3389/fnagi.2017.00117
49. Nir TM, Jahanshad N, Villalon-Reina JE, et al. Effectiveness of regional DTI measures in distinguishing Alzheimer's disease, MCI, and normal aging. *Neuroimage Clin*. 2013;3:180-195. doi:10.1016/j.nicl.2013.07.006
50. Lin CP, Frigerio I, Bol JGJM, et al. Microstructural integrity of the locus coeruleus and its tracts reflect noradrenergic degeneration in Alzheimer's disease and Parkinson's disease. *Transl Neurodegener*. 2024;13(1):9. doi:10.1186/s40035-024-00400-5
51. Arendt T, Brückner MK, Morawski M, Jäger C, Gertz HJ. Early neurone loss in Alzheimer's disease: cortical or subcortical?. *Acta Neuropathol Commun*. 2015;3(1):10. doi:10.1186/s40478-015-0187-1
52. Aggleton JP, Nelson AJD, O'Mara SM. Time to retire the serial Papez circuit: implications for space, memory, and attention. *Neurosci Biobehav Rev*. 2022;140:104813. doi:10.1016/j.neubiorev.2022.104813
53. Langley J, Hussain S, Flores JJ, Bennett IJ, Hu X. Characterization of age-related microstructural changes in locus coeruleus and substantia nigra pars compacta. *Neurobiol Aging*. 2020;87:89-97. doi:10.1016/j.neurobiolaging.2019.11.016
54. Nelson PT, Alafuzoff I, Bigio EH, et al. Correlation of Alzheimer disease neuropathologic changes with cognitive status: a review of the literature. *J Neuropathol Exp Neurol*. 2012;71(5):362-381. doi:10.1097/NEN.0b013e31825018f7
55. Ossenkoppele R, Smith R, Mattsson-Carlgren N, et al. Accuracy of tau positron emission tomography as a prognostic marker in preclinical and prodromal Alzheimer disease: a head-to-head comparison against amyloid positron emission tomography and magnetic resonance imaging. *JAMA Neurol*. 2021;78(8):961-971. doi:10.1001/jamaneurol.2021.1858
56. Bejanin A, Schonhaut DR, La Joie R, et al. Tau pathology and neurodegeneration contribute to cognitive impairment in Alzheimer's disease. *Brain*. 2017;140(12):3286-3300. doi:10.1093/brain/awx243
57. Betts MJ, Cardenas-Blanco A, Kanowski M, et al. Locus coeruleus MRI contrast is reduced in Alzheimer's disease dementia and correlates with CSF Aβ levels. *Alzheimers Dement*. 2019;11:281-285. doi:10.1016/j.dadm.2019.02.001
58. Dordevic M, Müller-Fotti A, Müller P, Schmicker M, Kaufmann J, Müller NG. Optimal cut-off value for locus coeruleus-to-pons intensity ratio as clinical biomarker for Alzheimer's disease: a pilot study. *J Alzheimers Dis Rep*. 2017;1(1):159-167. doi:10.3233/ADR-170021
59. Takahashi J, Shibata T, Sasaki M, et al. Detection of changes in the locus coeruleus in patients with mild cognitive impairment and Alzheimer's disease: high-resolution fast spin-echo T1-weighted imaging. *Geriatr Gerontol Int*. 2015;15(3):334-340. doi:10.1111/ggi.12280
60. Hou R, Beardmore R, Holmes C, Osmond C, Darekar A. A case-control study of the locus coeruleus degeneration in Alzheimer's disease. *Eur Neuropsychopharmacol*. 2021;43:153-159. doi:10.1016/j.euroneuro.2020.12.013
61. Tona KD, van Osch MJP, Nieuwenhuis S, Keuken MC. Quantifying the contrast of the human locus coeruleus in vivo at 7 Tesla MRI. *PLoS ONE*. 2019;14(2):e0209842. doi:10.1371/journal.pone.0209842
62. Jones DK, Knösche TR, Turner R. White matter integrity, fiber count, and other fallacies: the do's and don'ts of diffusion MRI. *Neuroimage*. 2013;73:239-254. doi:10.1016/j.neuroimage.2012.06.081

63. Albi A, Pasternak O, Minati L, et al. Free water elimination improves test–retest reproducibility of diffusion tensor imaging indices in the brain: a longitudinal multisite study of healthy elderly subjects. *Hum Brain Mapp*. 2017;38(1):12-26. doi:10.1002/hbm.23350
64. Golub M, Neto Henriques R, Gouveia Nunes R. Free-water DTI estimates from single b-value data might seem plausible but must be interpreted with care. *Magn Reson Med*. 2021;85(5):2537-2551. doi:10.1002/mrm.28599

SUPPORTING INFORMATION

Additional supporting information can be found online in the Supporting Information section at the end of this article.

How to cite this article: Aiello M, Marizzoni M, Borrelli P, et al. Microstructural assessment of the locus coeruleus–entorhinal cortex pathway and association with ATN markers in cognitive impairment. *Alzheimer's Dement*. 2025;21:e70126. https://doi.org/10.1002/alz.70126